Hafnium implanted in iron. II. Isolated hafnium-nitrogen complexes

1993 J. Phys.: Condens. Matter 5 2181

(http://iopscience.iop.org/0953-8984/5/14/015)

J. Phys.: Condens. Matter 5 (1993) 2181–2194. Printed in the UK

Hafnium implanted in iron: II. Isolated hafnium–nitrogen complexes

J M G J de Bakker and F Pleiter

Vakgroep Nucleaire Vaste Stof Fysica, Rijksuniversiteit Groningen, Nijenborgh 4, 9747 AG Groningen, The Netherlands

Received 24 August 1992, in final form 2 December 1992

Abstract. We have used the perturbed angular correlation technique to study the interaction of interstitially diffusing nitrogen atoms with substitutional hafnium atoms implanted in iron. It was found that after post-implantation of 250 eV nitrogen ions at 450 K, isolated $HfVN_x$ complexes with $x = 1, 2$ are formed in the iron matrix. We propose a possible geometrical configuration for the $HfVN_2$ complex. Isochronal annealing experiments showed nitrogen dissociation from the $HfVN_x$ complexes at 773 K. The dissociation energy was determined to be 2.7(2) eV.

1. Introduction

For many years now, internal nitriding of iron-based alloys has been widely applied because of its great technological importance. The production of a dispersion of small particles of alloying elements and dissolved nitrogen atoms in the matrix results in improvement of fatigue and of tribological and anticorrosion properties (Kane 1970). Electron microscopy, transmission electron microscopy and x-ray diffraction are the techniques most frequently used to study the formation, stability and microstructure of the nitride particles. However, with these techniques it is not possible to obtain information about the initial stage during which atomic-sized complexes of interstitial nitrogen atoms and (substitutional) solute atoms are formed, prior to the formation of larger clusters and/or precipitates. Hyperfine interaction techniques such as Mössbauer spectroscopy and perturbed angular correlation (PAC) have been shown to be very powerful in the study of simple complexes of solute and gas atoms (Wrede *et al* 1986, Andreasen *et al* 1989, Segeth *et al* 1989). We have applied the latter technique to study the formation of isolated hafnium–nitrogen complexes in the iron matrix. The results of our investigations are presented in this paper. The reader is referred to the paper by Fransens *et al* (1991) for a short description of the essential features of the PAC technique. A more complete treatment on this subject can be found in the work of Frauenfelder and Steffen (1965) and Wichert and Recknagel (1985).

2. Experimental details

Iron single crystals and polycrystalline foils were implanted at room temperature with 110 keV radioactive ^{181}Hf ions to doses between 2×10^{12} and 3×10^{14} atoms cm^{-2}.

0953-8984/93/142181+14$07.50

The single-crystal surfaces were parallel to a {211} or {100} crystallographic plane. Details of the crystals are given in the preceding paper (hereafter referred to as I). The iron foils were cut from a batch of 25 μm thickness and 99.998% purity (metallic impurities only). Before the implantation, the foils were degreased with acetone and annealed for 1 h at 700 °C in a flow of dry H_2 to reduce a possible surface oxide layer.

We post-implanted 500 eV $^{15}N_2^+$ ions, corresponding to 250 eV $^{15}N^+$ ions, into the samples. When selecting the energy of the nitrogen ions, a compromise had to be made: on the one hand, the penetration depth of the ions should be sufficiently large and, on the other hand, the probability for additional damage production in the host lattice should be sufficiently small. The implanted doses ranged from 1×10^{14} to 1×10^{17} atoms cm^{-2}. The pressure in the implantation chamber was less than 5×10^{-8} mbar and the ion current was usually of the order of 250 nA cm^{-2}. The implantation temperature was 450 K.

All foils and one of the single crystals were given isochronal annealing treatments. Each step lasted 20 min and was carried out in vacuum, at pressures of less than 10^{-6} mbar and 5×10^{-8} mbar for the foils and the crystals, respectively.

After each (post-)implantation and after each annealing treatment, the PAC of the 133–482 keV $\gamma\gamma$ cascade of the daughter nucleus ^{181}Ta was measured, as described in I. The sample was always at room temperature, in a magnetizing field of 0.17 T. The magnetization direction was either perpendicular to the plane of the detectors or in this plane at an angle of 45° to the detectors. The orientations of the samples with respect to the detectors and the magnetization directions are listed in table 1.

Table 1. Measuring geometry applied in the PAC experiments presented in this paper, where the angles θ and ϕ are defined with respect to the main crystallographic axes (see appendix): ||, magnetization parallel to detector plane; ⊥, magnetization perpendicular to detector plane.

Magnetization direction		Detector angles (θ, ϕ)				Crystal surface	
[hkl]	|| or ⊥	1	2	3	4	(hkl)	Figure
[110]	||	(122, 258)	(122, 12)	(58, 78)	(58, 192)	(211)	1
[110]	||	(122, 258)	(122, 12)	(58, 78)	(58, 192)	(211)	2
[001]	⊥	(90, 45)	(90, 135)	(90, 225)	(90, 315)	(100)	4(*a*)
[222]	⊥	(122, 258)	(122, 12)	(58, 78)	(58, 192)	(211)	4(*b*)
[110]	⊥	(94, 315)	(176, 135)	(86, 135)	(4, 315)	(211)	4(*c*)
[110]	||	(122, 258)	(122, 12)	(58, 78)	(58, 192)	(211)	5
–	||	–	–	–	–	Random	6(*a*)
–	⊥	–	–	–	–	Random	6(*b*)

The nitrogen depth profile was measured using the resonant nuclear reaction $^{15}N(p, \alpha\gamma)^{12}C$ with $E_p = 429$ keV and $\Gamma = 120(30)$ eV (Maurel and Amsel 1983). We used a 4 in × 4 in NaI γ-ray detector placed at a back-scattering angle of about 130°. The proton beam was incident perpendicular to the crystal surface. The depth distribution was obtained by measuring the yield of emitted γ-rays as a function of incident proton beam energy and deconvoluting this yield, using a Lorentzian response curve with a width of 0.5 keV FWHM (Smulders 1986).

3. Results

Figures 1(*a*) and 1(*b*) show normalized Fourier transforms of PAC spectra measured before and after post-implantation of 4×10^{16} nitrogen atoms cm^{-2}, respectively. In figure 1(*a*), one observes a single magnetic Larmor frequency $\omega_B = 3.80(2)$ Grad s^{-1}, which is attributed to substitutional Hf atoms in a damage-free cubic environment (I). In figure 1(*b*), a series of hyperfine interaction frequencies below ω_B has appeared at the expense of the substitutional peak. It is evident that these frequencies are induced by nitrogen association of the substitutional hafnium probe atoms.

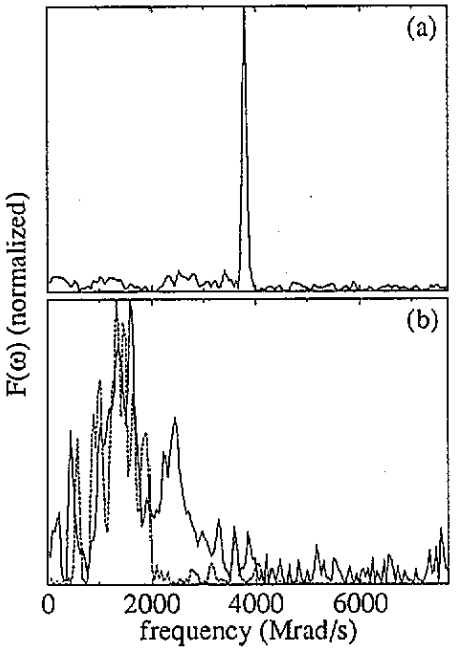

Figure 1. Normalized Fourier spectra measured on ^{181}HfFe: (*a*) as implanted; (*b*) after post-implantation at 450 K of 250 eV nitrogen to a dose of 4×10^{16} atoms cm^{-2}. The broken curve in (*b*) was calculated using the hyperfine parameters given in (1) and (2). The measuring geometry is given in table 1.

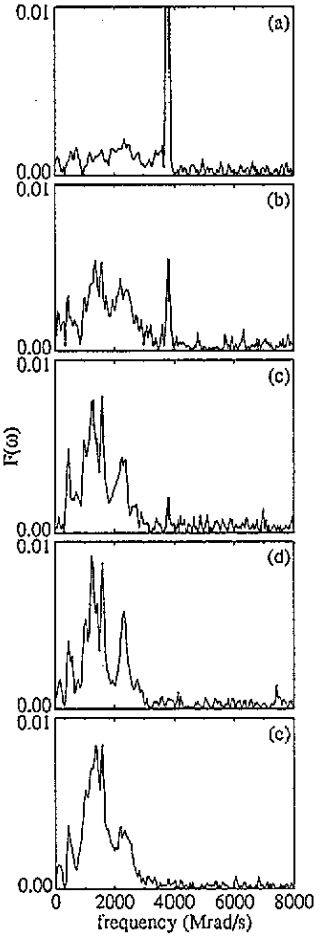

Figure 2. Fourier transforms of PAC spectra measured on the system ^{181}HfFe, post-implanted at 450 K with 250 eV nitrogen to doses of (*a*) 1.7×10^{16} atoms cm^{-2}, (*b*) 2.7×10^{16} atoms cm^{-2}, (*c*) 3.2×10^{16} atoms cm^{-2}, (*d*) 3.7×10^{16} atoms cm^{-2} and (*e*) 3×10^{17} atoms cm^{-2}. The measuring geometry is given in table 1.

Two major questions arise about the nitrogen-induced interaction frequencies. Firstly are these frequencies due to a single hyperfine interaction or are they a

superposition of frequencies originating from more than one interaction? Secondly what is the nature (electric, magnetic or combined) of the hyperfine interaction(s) leading to the observed frequencies?

In order to find an answer to the first question, we have performed a series of successive nitrogen post-implantations and PAC measurements. In figure 2, we show Fourier spectra measured after nitrogen post-implantation to integrated doses varying from 1.7×10^{16} to 3×10^{17} atoms cm^{-2}. With increasing dose, the substitutional fraction f_s, first changes from 25.7(3)% in the as-implanted sample to 34.5(3)% at a dose of 2×10^{15} atoms cm^{-2} and then to 20.0(4)% at a dose of 1.7×10^{16} atoms cm^{-2}. Up to this dose no clearly distinguishable new frequencies appear in the Fourier transform. After implantation of 2.7×10^{16} atoms cm^{-2}, f_s suddenly has decreased to less than 5% while simultaneously a set of new interaction frequencies shows up in the Fourier transform. These frequencies grow to their maximum amplitudes during implantation to a dose of 3.2×10^{16} atoms cm^{-2}. At a nitrogen dose of 3.7×10^{16} atoms cm^{-2}, f_s is zero. Up to the highest dose of 3×10^{17} atoms cm^{-2} the frequency spectrum does not show any significant changes.

The small increase in f_s is attributed to detrapping of lattice defects from non-substitutional probe nuclei due to the elevated sample temperature during the nitrogen implantation. The fact that *all* the new frequencies appear *simultaneously* suggests that only a single hyperfine interaction is responsible for the whole set of frequencies. The strong decrease in f_s *before* the appearance of the set of new frequencies and the fact that these frequencies do not change at higher doses suggest that we are dealing with at least two different hafnium–nitrogen configurations. Presumably, a HfVN† complex with one nitrogen atom is formed at low doses while at higher doses this complex is transformed to a single, stable and well defined $HfVN_x$ complex with $x \geqslant 2$. A possible reason why the interaction frequencies of the initial HfVN complex do not show up in the Fourier transform is that this complex occurs in a variety of (slightly) different configurations, causing the interaction frequencies to be smeared out over a broad frequency range.

In figure 3 we show the nitrogen depth distribution after having implanted a dose of about 3×10^{17} atoms cm^{-2}. A significant fraction of the implanted nitrogen atoms are located in the near-surface region at a depth much smaller than the average range of the implanted Hf atoms (I). This demonstrates that Hf atoms do not form the dominant trapping centres for nitrogen (see also discussion).

In order to be able to answer the second question, we post-implanted a nitrogen dose of 4×10^{16} atoms cm^{-2} into several single crystals and performed PAC measurements for different geometries. In figure 4 we show three Fourier spectra recorded with the crystal magnetized in a direction perpendicular to the detector plane, but with different crystal orientations with respect to the detectors (table 1). Comparing the spectra measured with the magnetization direction perpendicular (figure 4) and parallel (figure 1(*b*)) to the plane of the detectors, we must conclude that we are dealing with combined magnetic and electric hyperfine interactions. If the interaction were purely magnetic, then the frequencies would just shift to the double value when changing the magnetization direction from parallel to perpendicular to the detector plane. If the interaction were purely electric, then the frequencies would be independent of the magnetization direction and only the amplitudes would change

† We denote a substitutional Hf atom by HfV, where V stands for a vacancy.

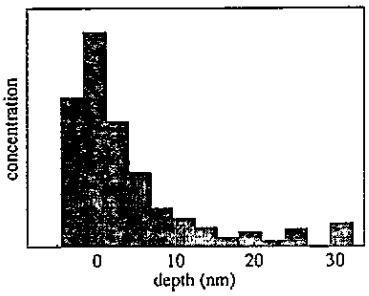

Figure 3. Depth profile of 250 eV N implanted in an Fe single crystal, determined using the resonant nuclear reaction $^{15}N(p, \alpha\gamma)^{12}C$ with $E_p = 429$ keV.

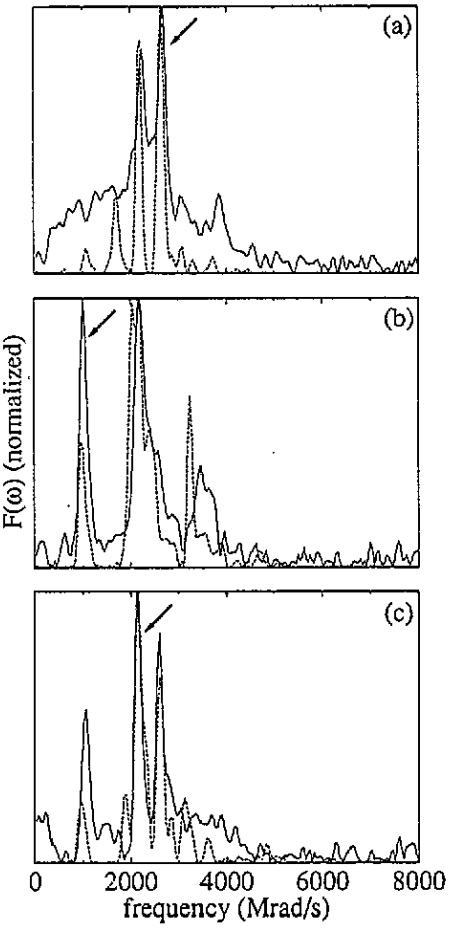

Figure 4. Experimental (——) and simulated (- - - -) Fourier transforms $F(\omega)$ of PAC spectra $R(t)$ for the system ^{181}HfNFe and different geometries (see table 1).

as a function of the orientation of the crystal with respect to the detectors (figure 4). Clearly, none of these is the case here. We determined the relative magnitudes and orientations of the electric field gradient (EFG) and the magnetic hyperfine field as well as the EFG asymmetry parameter η using the spectra shown in figure 4. We proceeded as follows.

For the measuring geometry in figure 4(b), we calculated the PAC function (see appendix) for a large number of values of the asymmetry parameter η, the ratio ω_0/ω_B of the electric and magnetic interaction frequencies and for different orientations of the EFG principal axes system. We started with 21 values of η between 0 and 1, and 47 values of ω_0/ω_B between 0.2 and 2.5. The direction of the EFG principal z axis was confined to the region delimited by the [001], [011] and [111] crystallographic directions. Given the symmetry properties of the BCC crystal, this region represents the whole space. The absolute magnitudes of ω_0 and ω_B were determined by stretching or compressing each calculated correlation function such that the frequency with the largest amplitude overlapped the measured frequency at

$\omega = 2.180$ Grad s^{-1}†. After this stage each set of parameters was tested for the first time with respect to its validity. For this, we checked whether a calculated frequency was present in a small region around the measured frequency at 1.002 Grad s^{-1} (indicated with an arrow in figure 4(*b*)), with a relative amplitude of at least 50%. When this was not the case, the parameter set was rejected. With the accepted sets of hyperfine interaction parameters, the correlation function was calculated for the geometries shown in figures 4(*a*) and 4(*c*). For each of these spectra, a test as described before was performed on the interaction parameters. The parameters were retained when the calculated spectra contained frequency components in small regions around the major frequencies indicated with arrows in figures 4(*a*) and 4(*c*), again with a relative amplitude of at least 50%. The goodness of fit was visually checked by comparing the calculated and measured Fourier transforms of the correlation functions, taking into account the finite time resolution of the detectors. The parameters were rejected when frequencies with a relatively large amplitude appeared at positions were none had been measured. Once an acceptable set of parameters was found, we gradually decreased the step and grid sizes for the variables η and ω_0/ω_B. In the last stages, the y axis of the EFG was rotated over 360° in steps of 10° around the retained z axes.

The hyperfine parameters that give the best fit to the measured spectra are

$$\omega_B = 1.14 \text{ Grad } s^{-1}$$
$$\omega_0 = 0.50 \text{ Grad } s^{-1} \tag{1}$$
$$\eta = 0.20.$$

The corresponding crystallographic directions of the principal z and y axes are

$$z: [2\,1\,\bar{1}0]$$
$$y: [\bar{1}\,2\,0]. \tag{2}$$

The Fourier transforms obtained with these parameters are shown as broken curves in figure 4. The experimental peak positions and amplitudes are reasonably well reproduced by the simulations.

As a further check on the parameter set (1) and (2), we calculated the correlation function for the geometry given in table 1 for figure 1(*b*). The result, shown as a broken curve in this figure, is quite acceptable. It is clear, however, that there is significant Fourier power in the measured spectrum in the region 2–3 Grad s^{-1}, which is not reproduced in the theoretical spectrum. Figure 2 shows that this Fourier power grows together with the peaks below 2 Grad s^{-1}. This suggests that, apart from the unique $HfVN_x$ complex with $x \geqslant 2$ mentioned at the beginning of this section, more hafnium–nitrogen complexes are formed, which are not described by the parameter set (1) and (2).

To investigate the thermal stability of the $HfVN_x$ complex, we have performed an isochronal annealing treatment on a crystal post-implanted with nitrogen to a dose of 4×10^{16} atoms cm^{-2}. Figures 5(*a*), 5(*b*), 5(*c*) and 5(*d*) show PAC spectra and corresponding Fourier transforms measured after nitrogen post-implantation at

† The amplitude of this frequency is attenuated by a factor $\gamma = 82\%$ because of the finite time resolution of the detectors. This implies that this peak has a real amplitude which is certainly larger than that at 1.002 Grad s^{-1}.

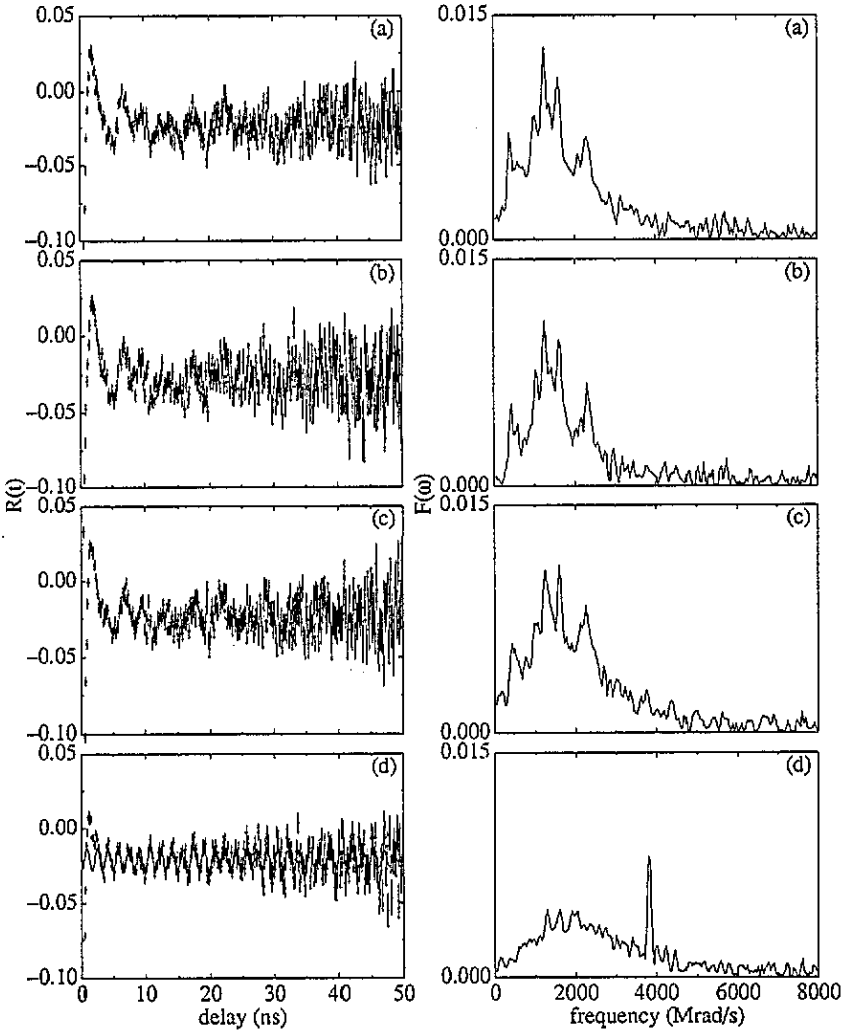

Figure 5. PAC spectra and corresponding Fourier transforms measured on an iron single crystal post-implanted with nitrogen to a dose of (*a*) 4×10^{16} atoms cm^{-2}, and annealed at (*b*) 563 K, (*c*) 673 K and (*d*) 773 K.

450 K, after annealing at 563 K, after annealing at 673 K and after annealing at 773 K, respectively. Figures 5(*a*)–5(*c*) show the spectrum characteristic of $HfVN_x$ formation and prove that the $HfVN_x$ complex is stable up to 673 K. After annealing at 773 K, most $HfVN_x$ complexes have dissociated and the initial substitutional fraction is restored to about 20% of the initial value.

As a final test of the hyperfine parameters, we have performed PAC measurements on an iron foil that had been post-implanted with nitrogen to a dose of 8×10^{16} atoms cm^{-2}. Measured and calculated $R(t)$ and $F(\omega)$ spectra are shown in figure 6. The agreement between theory and experiment is very reasonable, especially if one bears in mind that the interaction parameters were kept fixed at the values (1) obtained from the single-crystal measurements. The only free parameter was the overall intensity. The substitutional component (labelled by S in figure 6) and the

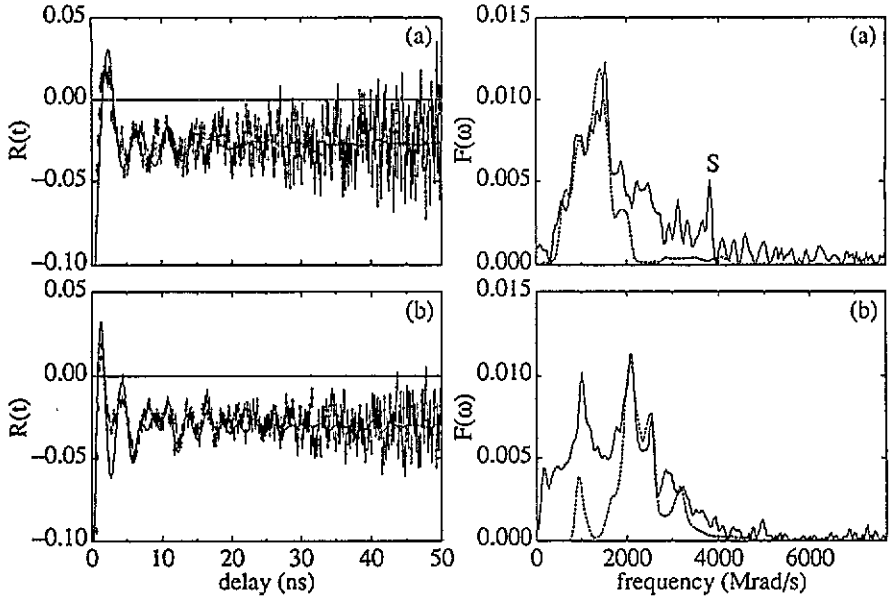

Figure 6. Theoretical (----) and experimental (——) spectra $R(t)$ and corresponding Fourier transforms $F(\omega)$ in the case of combined interaction in a polycrystalline iron sample. The hyperfine interaction parameters are $\omega_B = 1.14$ Grad s^{-1}, $\omega_0 = 0.50$ Grad s^{-1} and $\eta = 0.20$. The peak labelled S is associated with substitutional Hf atoms. The measuring geometry is given in table 1.

component which causes the broadly distributed Fourier power are not included in the fit. The latter component shows up in the time domain (left-hand side of figure 6) as a rapid change in the anisotropy at time zero; it is in part an artefact which is caused by differences in time response of the four detector systems. In the following we shall discuss the foil experiments in somewhat more detail.

Post-implantation with a nitrogen dose of 4×10^{16} atoms cm^{-2} resulted in an increase in f_s from about 17.4(4)% to 29.5(5)%. This is in contrast with the single-crystal measurements where this dose was sufficient to decorate all the substitutional ^{181}Hf probe atoms. After implantation of an additional dose of 4×10^{16} atoms cm^{-2}, f_s decreased to 16.9(4)%, but still no new frequencies appeared in the Fourier transform. This suggests that most nitrogen atoms implanted in the foils are trapped in the subsurface layer before diffusing towards the hafnium probe atoms implanted at larger depths. It is known that an oxide layer of 5–7 nm thickness forms immediately on iron foils upon exposure to air. We were not able to prevent oxidation of our films prior to the nitrogen implantations. Thus, we expect that virtually all the implanted nitrogen has come to rest in an oxide layer where it is immobilized at the implantation temperature. To release the nitrogen atoms from this layer, we have annealed the samples at 573 and 673 K. After the first annealing step, f_s decreased to 11.0(6)% and a broad distribution of frequencies around 1.5 Grad s^{-1} began to appear. After annealing at 673 K, f_s was almost zero and the spectrum shown in figure 6(*a*) was measured. Apparently, at this temperature some of the nitrogen atoms trapped in the oxide layer have diffused into the crystal where they have been retrapped at the Hf probes.

4. Discussion

N^+ ions, implanted in iron with an energy of 250 eV, come to rest in a subsurface region extending to a depth of about 3 nm. According to a TRIM (Biersack and Haggmark 1980) calculation, less than 1% of the 110 keV Hf atoms have landed in this region. The diffusion coefficient of interstitial nitrogen in iron at 450 K is $D = 5 \times 10^{-12}$ cm^2 s^{-1} (Fromm and Gebhardt 1976). This means that interstitial nitrogen is highly mobile at the implantation temperature. Thus, during the implantation, nitrogen atoms will thermally diffuse out of the subsurface region, either towards the crystal surface or into the bulk, until they become trapped. Those diffusing into the crystal may be trapped at hafnium atoms or at other competing trapping centres such as implantation damage or, in the case of Fe foils, grain boundaries. In our PAC measurements, we have clearly observed that a fraction of the implanted nitrogen escapes from the subsurface layer into the crystal where it is trapped at substitutional Hf in the iron matrix. This was confirmed by an NRA measurement which showed nitrogen to be present beyond the nitrogen implantation range.

The NRA measurement also revealed a large nitrogen concentration in the subsurface region. By means of conversion-electron Mössbauer spectroscopy, it has been observed that precipitation of the iron nitrides ϵ-Fe_2N, ϵ-Fe_3N and γ'-Fe_4N occurs after implantation of 50 keV nitrogen in Fe at 20 and 200 °C to doses of 5×10^{16}–5×10^{17} atoms cm^{-2} (Terwagne *et al* 1989). Therefore, we think that iron nitrides have formed in the subsurface region of our samples. These precipitates are invisible in the PAC measurements since the implanted hafnium probe atoms are located at much larger depths.

HfN_x formation has been observed before in the BCC metals Nb and Ta (Mendes *et al* 1988). For N-loaded Ta, these workers observed only one quadrupole interaction frequency, whereas three interactions—one of which is clearly dominant—were necessary to describe the experimental results for Nb. The single or dominant interaction frequency was attributed to trapping of a single N atom by the Hf probe. The remaining frequencies in Nb were assumed to arise from several types of defect with different numbers of trapped N atoms. We shall now discuss the $HfVN_x$ complex in iron, characterized by the hyperfine interaction parameters (1) and (2), in more detail.

It is known from channelling measurements that free nitrogen in the α-iron matrix is located at octahedral or near-octahedral interstitial sites (Swanson *et al* 1985). From the infrared spectrum of gaseous HfN molecules, a value of 1.69(3) Å has been derived for the equilibrium internuclear distance in this molecule (DeVore and Gallaher 1979). This distance is only slightly larger than the distance of 1.433 Å between a regular lattice site and a nearest octahedral interstitial site. Our PAC measurements show that the principal z axis of the nitrogen-induced EFG is approximately parallel to a ⟨001⟩ crystallographic direction and that the asymmetry parameter is small but non-zero. Additionally, from the sequence of PAC spectra measured as a function of nitrogen dose (figure 2), it follows that a single substitutional Hf atom and more than one nitrogen atom is involved in the formation of the considered $HfVN_x$ complex. Taking all these data together, a possible configuration for the $HfVN_x$ complex consists of a substitutional Hf atom associated with two interstitial nitrogen atoms located at nearest octahedral sites: $HfVN_2$. The non-zero asymmetry parameter is easily reproduced by the point-charge model if both N atoms are slightly displaced from their perfect octahedral sites, such that both Hf–N

bonds make an angle that is slightly larger or smaller than 90°. The EFG is then oriented in a ⟨001⟩ direction perpendicular to the plane through the Hf and N atoms.

After annealing at 773 K, the signal characteristic for the $HfVN_2$ complex was found to have almost disappeared while the signal characteristic for substitutional Hf atoms was found to be partially restored. At this temperature, Hf is virtually immobile in Fe compared with interstitial nitrogen (I). From these data, we conclude that nitrogen desorbs at 773 K from the $HfVN_2$ as well as from the HfVN complex. Assuming a single-step detrapping process, we can calculate the energy needed to dissociate a nitrogen atom from a $HfVN_x$ complex with $x = 1, 2$ from the expression

$$E^{dis}_{HfVN_x} = k_B T^{dis}_{HfVN_x} \ln(\nu_0 t / \ln 2) \tag{3}$$

where $t = 1200$ s is the annealing time and ν_0 is the attempt frequency. This frequency can be derived from the following expression for the diffusion coefficient D_0, for jumps between octahedral sites in a BCC lattice (Schultz 1968–9)

$$D_0 = \tfrac{1}{24} a^2 \nu_0 \tag{4}$$

where a is the lattice constant. Using the value $D_0 = 7.8 \times 10^{-3}$ cm^2 s^{-1} (Fromm and Gebhardt 1976), we find $\nu_0 = 4.6 \times 10^{14}$ s^{-1}. Taking $T^{dis}_{HfVN_x} = 773(50)$ K as the temperature at which the fraction of $HfVN_x$ complexes is reduced by 50%, we get $E^{dis}_{HfVN_x} = 2.7(2)$ eV for the dissociation energy of $HfVN_x$ complexes with $x = 1, 2$ in α-iron. Using a value of $E^m_N = 0.76$ eV (Schultz 1968–9) for the migration energy of N in α-iron, we obtain a nitrogen binding energy of $E^b_{HfVN_x} = 1.9(2)$ eV from the relation

$$E^{dis}_{HfVN_x} = E^b_{HfVN_x} + E^m_N. \tag{5}$$

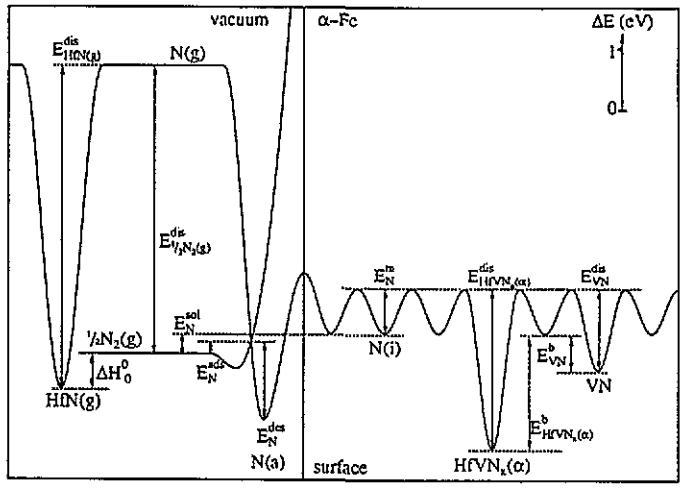

Figure 7. Energy diagram of the nitrogen–iron and nitrogen–hafnium interactions (see text).

Figure 7 shows a quantitative energy diagram of the nitrogen–iron and nitrogen–hafnium interactions. Experimental activation energies and enthalpies are listed in

table 2. In the vacuum, gaseous nitrogen forms a molecule, $N_2(g)$. The energy required to dissociate a hafnium–nitrogen pair in vacuum is

$$E^{dis}_{HfN(g)} = E^{dis}_{(1/2)N_2(g)} + \Delta H_0{}^\circ \tag{6}$$

with $E^{dis}_{(1/2)N_2(g)}$ being half the dissociation energy of a nitrogen molecule and $\Delta H_0{}^\circ$ being the standard reaction enthalpy at 0 K for the reaction

$$HfN(g) = Hf(g) + \tfrac{1}{2}N_2(g). \tag{7}$$

Upon approaching the crystal surface N_2 molecules dissociate and become chemisorbed as atoms, N(a). The reverse reaction $N(a) \rightarrow \frac{1}{2}N_2(g)$ requires an activation energy E^{des}_N. The activation energy E^{ads}_N for chemisorption and the activation energy E^{des}_N for desorption depend on the crystal surface structure. The formation energy of an interstitial nitrogen atom N(i) in the bulk, or the heat of solution, is denoted by E^{sol}_N. The migration energy is given by E^{m}_N. The dissociation energy of a nitrogen–vacancy pair is denoted by E^{dis}_{VN}.

Table 2. Energies involved in the interactions of nitrogen with iron and hafnium.

Parameter	Value (eV)	Reference
E^{ads}_N	0.1 (100) 0.15 (110) 0.0 (111)	Bozso *et al* (1977a, b)
E^{des}_N	1.3 (100) 1.2 (110) 1.1 (111)	Bozso *et al* (1977a, b)
$E^{dis}_{(1/2)N_2(g)}$	4.9(1)	Kohl and Stearns (1974)
$E^{dis}_{HfN(g)}$	5.5(3)	Kohl and Stearns (1974)
$\Delta H_0{}^\circ$	0.6(3)	Kohl and Stearns (1974)
E^{m}_N	0.76	Schultz (1968–9)
$E^{dis}_{HfVN_x(\alpha)}$	2.7(2)	This work
$E^{b}_{HfVN_x(\alpha)}$	1.9(2)	This work
E^{dis}_{VN}	1.4	Weller and Diehl (1976)
E^{sol}_N	0.4	Fromm and Gebhardt (1976)

The Hf–nitrogen dissociation energy $E^{dis}_{HfVN_x} = 2.7(2)$ eV, is considerably smaller than the corresponding value for the gas phase, $E^{dis}_{HfN(g)} = 5.5(3)$ eV, but much larger than the depth of the potential well, $E^{m}_N = 0.76$ eV, for interstitial nitrogen (see table 2 and figure 7). Therefore the chemical bond between Hf and N in α-iron seems still to exist, although much reduced compared with the gas phase.

5. Conclusion

By means of PAC experiments on the system ^{181}HfNFe we have observed the formation and dissociation of isolated $HfVN_x$ complexes with $x = 1, 2$ in iron. The nitrogen dissociation energy from these complexes was determined to be 2.7(2) eV. We propose a possible geometrical configuration for the complex $HfVN_2$.

Acknowledgments

This work was performed as a part of the research programme of the Stichting voor Fundamenteel Onderzoek der Materie, with financial support from the Nederlandse Organisatie voor Wetenschappelijk Onderzoek.

Appendix. Perturbation function in the case of static combined interactions

Consider a radioactive nucleus with the initial state $|I_i m_i\rangle$ that decays to an intermediate state $|Im\rangle$ by emitting a γ-quantum k_1 with multipolarities L_1 and L_1' in the direction (θ_1, ϕ_1). After a time t, the nucleus decays to the ground state $|I_f m_f\rangle$ by emitting a second γ-quantum k_2, with multipolarities L_2 and L_2', in the direction (θ_2, ϕ_2). If the nucleus in its intermediate state interacts with extranuclear electric and/or magnetic fields, the γ–γ angular correlation function becomes time dependent (Frauenfelder and Steffen 1965)

$$W(\boldsymbol{k}_1, \boldsymbol{k}_2, t) = \sum_{\substack{N_1 N_2 \\ k_1 k_2}} A_{k_1}(1) A_{k_2}(2) G_{k_1 K_2}^{N_1 N_2}(t) [(2k_1 + 1)(2k_2 + 1)]^{-1/2} \times Y_{k_1}^{N_1 *}(\theta_1, \phi_1) Y_{k_2}^{N_2}(\theta_2, \phi_2) \tag{A1}$$

with k_i an even integer, $0 \leqslant k_i \leqslant \min(2I, L_i + L_i')$ and $|N_i| \leqslant k_i$. $W(\boldsymbol{k}_1, \boldsymbol{k}_2, t)\, \mathrm{d}\Omega_1\, \mathrm{d}\Omega_2$ is defined as the probability that the γ-quanta k_1 and k_2 are emitted into the solid angles $\mathrm{d}\Omega_1$ and $\mathrm{d}\Omega_2$, respectively. The functions $Y_k^N(\theta, \phi)$ represent normalized spherical harmonics. The values of the anisotropy coefficients A_{k_1} and A_{k_2} are determined by the spin values involved in the nuclear cascade and the multipolarities of the two consecutive γ-ray transitions. They can be calculated from the tabulated F-coefficients (Frauenfelder and Steffen 1965). The influence of the extranuclear perturbation is completely described by the perturbation function $G_{k_1 k_2}^{N_1 N_2}(t)$. As long as only static fields are considered, this perturbation function is given by

$$G_{k_1 k_2}^{N_1 N_2}(t) = \sum_{\substack{m_a m_b \\ n n'}} (-1)^{2I + m_a + m_b} [(2k_1 + 1)(2k_2 + 1)]^{1/2} \exp\left(-\frac{\mathrm{i}}{\hbar}(E_n - E_{n'})t\right) \times \langle n|m_b\rangle^* \langle n|m_a\rangle \langle n'|m_b'\rangle \langle n'|m_a'\rangle^* \times \begin{pmatrix} I & I & k_1 \\ m_a' & -m_a & N_1 \end{pmatrix} \begin{pmatrix} I & I & k_2 \\ m_b' & -m_b & N_2 \end{pmatrix} \tag{A2}$$

where the last two factors are Wigner 3_j symbols. The eigenvectors $\langle m|n\rangle$ and eigenvalues E_n are obtained by diagonalizing the interaction Hamiltonian **H** which describes the perturbation in question (Alder *et al* 1963):

$$\mathbf{UHU}^{-1} = \mathbf{E} \tag{A3}$$

where **E** is the diagonal energy matrix with elements E_n and the $\langle m|n\rangle$ are the matrix elements of the unitary matrix **U**.

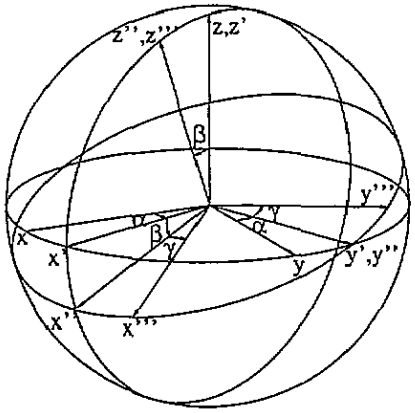

Figure A1. Euler angles α, β and γ which define the rotation from the Cartesian coordinate system (x, y, z) towards the system (x''', y''', z''').

If the nuclear probe is subjected to a static combined magnetic dipole and electric quadrupole interaction, then **H** can be written as the sum of $\mathbf{H}_B$ and $\mathbf{H}_E$, where $\mathbf{H}_B$ describes the interaction of the nuclear magnetic dipole moment μ with the magnetic field B, and $\mathbf{H}_E$ describes the interaction of the nuclear electric quadrupole moment Q with the electric field gradient. In order to calculate the matrix elements of the total interaction Hamiltonian **H**, we introduce a laboratory system $S(x, y, z)$ and the systems $S_B(x, y, z)$ and $S_E(x, y, z)$ in which $\mathbf{H}_B$ and $\mathbf{H}_E$, respectively, are diagonal. Let the Euler angles α_B, β_B and γ_B (α_E, β_E and γ_E) define the rotation from S_B (S_E) towards S. The convention used in the choice of the Euler angles is shown in figure A1. The matrix elements $H_{mm'}$ of the interaction Hamiltonian in the system S are obtained after transformation of $\mathbf{H}_B$ ($\mathbf{H}_E$) from S_B (S_E) to the laboratory system. They can be written as (Matthias *et al* 1963, Boström *et al* 1970)

$$\begin{aligned}
H_{mm} &= \omega_B \hbar m \cos\beta_B + \omega_E \hbar \tfrac{1}{2}[3\cos^2\beta_E - 1 + \eta \sin^2\beta_E \cos(2\alpha_E)] \\
&\quad \times [3m^2 - I(I+1)] \\
H_{mm\pm1} &= \tfrac{1}{2}\hbar\omega_B[I(I+1) - m(m\pm1)]^{1/2} \sin\beta_B \exp(\pm i\gamma_B) \\
&\quad + \tfrac{3}{2}\omega_E \hbar \sin\beta_E \{\cos\beta_E \mp \tfrac{1}{6}\eta[(1 \pm \cos\beta_E)\exp(2i\alpha_E) - (1 \mp \cos\beta_E) \\
&\quad \times \exp(-2i\alpha_E)]\} \exp(\pm i\gamma_E)(2m \pm 1)[(I \mp m)(I \pm m + 1)]^{1/2} \qquad \text{(A4)} \\
H_{mm\pm2} &= \omega_E \hbar \tfrac{3}{4}\{\sin^2\beta_E + \tfrac{1}{6}\eta[(1 \pm \cos\beta_E)^2 \exp(2i\alpha_E) \\
&\quad + (1 \mp \cos\beta_E)^2 \exp(-2i\alpha_E)]\} \exp(\pm 2i\gamma_E)[(I \pm m + 2)(I \pm m + 1) \\
&\quad \times (I \mp m)(I \mp m - 1)]^{1/2}.
\end{aligned}$$

The magnetic Larmor frequency ω_B is defined as

$$\omega_B = -g_N \mu_N B/\hbar \tag{A5}$$

where g_N is the nuclear g-factor for the intermediate state and μ_N is the nuclear magneton. The electric quadrupole frequency ω_E is defined as

$$\omega_E = eQV_{zz}/4I(2I-1)\hbar \tag{A6}$$

where V_{zz} is the z component of the diagonalized EFG tensor. The deviation from axial symmetry of this tensor is given by the asymmetry parameter

$$\eta = (V_{xx} - V_{yy})/V_{zz} \tag{A7}$$

with $|V_{xx}| \leqslant |V_{yy}| \leqslant |V_{zz}|$ and $V_{xx} + V_{yy} + V_{zz} = 0$, which restricts η to $0 \leqslant \eta \leqslant 1$.

The intermediate state of ^{181}Ta has a nuclear spin $I = \frac{5}{2}$. For half-integer spin values, we have

$$\omega_0 = 6\omega_E. \tag{A8}$$

In this study, the probe nucleus ^{181}Hf was located in a cubic (BCC) ferromagnetic *single-crystal* or *polycrystalline* foil. In the PAC experiments, the crystal was magnetized in a well defined direction, either perpendicular to the plane of the detectors or in this plane at an angle of 45° with respect to the detectors. In the single-crystal case, we chose the orientation of the laboratory system $S(x, y, z)$ such that the positive x, y and z axes coincided with the [100], [010] and [001] crystallographic directions, respectively. The correlation function was calculated for all 24 equivalent crystallographic orientations of S_E and subsequently averaged. In the polycrystalline case, we averaged the correlation function for 10^4 randomly selected directions.

References

Alder K, Matthias E, Schneider W and Steffen R M 1963 *Phys. Rev.* **129** 1199

Andreasen H, Boerma D O, Niesen L, Segeth W and de Waard H 1989 *Hyperfine Interact.* **47** 69

Biersack J P and Haggmark L G 1980 *Nucl. Instrum. Methods* **174** 257

Boström L, Karlsson E and Zetterlund S 1970 *Phys. Scr.* **2** 65

Bozso F, Ertl G, Grunze M and Weiss M 1977a *J. Catal.* **49** 18

Bozso F, Ertl G and Weiss M 1977b *J. Catal.* **50** 519

DeVore T C and Gallaher T N 1979 *J. Chem. Phys.* **70** 3497

Fransens J R, Abd El Keriem M S and Pleiter F 1991 *J. Phys.: Condens. Matter* **3** 9871

Frauenfelder H and Steffen R M 1965 *Alpha-, Beta-, and Gamma-Ray Spectroscopy* vol 2, ed K Siegbahn (Amsterdam: North-Holland) ch XIXA

Fromm E and Gebhardt E 1976 *Gase and Kohlenstoff in Metallen* (Berlin: Springer)

Kane J S 1970 *Metall. Trans.* **1** 548

Kohl F J and Stearns C A 1974 *J. Phys. Chem.* **78** 273

Matthias E, Olsen B and Schneider W 1963 *Ark. Fys.* **24** 245

Maurel B and Amsel G 1983 *Nucl. Instrum. Methods* **218** 159

Mendes P J, Gil J M, Ayres De Campos N, De Lima A P and Weidinger A 1988 *Nuclear Physics Applications on Materials Science* ed E Recknagel and J C Soares (Deventer: Kluwer) p 269

Schultz H 1968–9 *Mater. Sci. Eng.* **3** 189

Segeth W, Boerma D O, Niesen L and Smulders P J M 1989 *Phys. Rev.* B **39** 10725

Smulders P J M 1986 *Nucl. Instrum. Methods* B **14** 234

Swanson M L, Howe L M, Jackman J A, Jackman T E, Griffiths K and Quenneville A F 1985 *Nucl. Instrum. Methods* B **7–8** 85

Terwagne G, Piette M, Bodart F and Möller W 1989 *Mater. Sci. Eng.* **A115** 25

Weller M and Diehl J 1976 *Scr. Metall.* **10** 101

Wichert Th and Recknagel E 1986 *Microscopic Methods in Metals (Topics in Current Physics 40)* ed U Gonser (Berlin: Springer) p 317

Wrede U, Schaefer T and Vianden R 1986 *Z. Phys.* B **64** 461